Multifunctional light escaping architecture inspired by compound eye surface structures: From understanding to experimental demonstration

Young Min Song,[1,*] Gyeong Cheol Park,[1] Sung Jun Jang,[1] Jong Hoon Ha,[1] Jae Su Yu,[2] and and Yong Tak Lee[1,3,4,5]

[1]*School of Information and Communications, Gwangju Institute of Science and Technology, 1 Oryong-dong, Buk-gu, Gwangju, 500-712, South Korea*
[2]*Department of Electronics and Radio Engineering, Kyung Hee University,1 Seocheon-dong, Giheung-gu, Yongin-si, Gyeonggi-do, 446-701, South Korea*
[3]*Graduate Program of Photonics and Applied Physics, Gwangju Institute of Science and Technology, 1 Oryong-dong, Buk-gu, Gwangju, 500-712 South Korea*
[4]*Department of Nanobio Electronics and Materials, Gwangju Institute of Science and Technology,1 Oryong-dong, Buk-gu, Gwangju, 500-712, South Korea*
[5]*ytlee@gist.ac.kr*
**ymsong@gist.ac.kr*

Abstract: We present bioinspired artificial compound eye surface structures that consist of antireflective subwavelength structures (SWSs) on hexagonally patterned microstructures (MSs), for the purpose of efficient light escaping inside light-emitting materials/devices. Theoretical understanding and geometrical optimization of SWSs on MSs are described together with rigorous coupled-wave analysis. As a proof of this concept, AlGaInP red light-emitting diodes (LEDs) with SWS/MSs were fabricated, and a light output power enhancement of 72.47% was achieved as compared to that of conventional LEDs. The artificial compound eye structures are not limited to LEDs, and the fabrication process is compatible with most semiconductor device manufacturing processes; hence, this concept opens up new possibilities for improving the optical performance of various optoelectronic device applications.

OCIS codes: (050.6624) Subwavelength structures; (220.4241) Nanostructure fabrication; (230.3670) Light-emitting diodes.

References and links

1. H. Ghiradella, "Structure and development of iridescent butterfly scales: lattices and laminae," J. Morphol. **202**(1), 69–88 (1989).
2. P. Vukusic, J. R. Sambles, C. R. Lawrence, and R. J. Wootton, "Structural colours: Now you see it – now you don't," Nature **410**(6824), 36 (2001).
3. W. Barthlott, and C. Neinhuis, "Purity of the sacred lotus, or escape from contamination in biological surfaces," Planta **202**(1), 1–8 (1997).
4. P. B. Clapham, and M. C. Hutley, ""Reduction of lens reflection by the "moth eye" principle," Nature **244**(5414), 281–282 (1973).
5. D. G. Stavenga, S. Foletti, G. Palasantzas, and K. Arikawa, "Light on the moth-eye corneal nipple array of butterflies," Proc. Biol. Sci. **273**(1587), 661–667 (2006).
6. L. P. Lee, and R. Szema, "Inspirations from biological optics for advanced photonic systems," Science **310**(5751), 1148–1150 (2005).
7. X. Gao, X. Yan, X. Yao, L. Xu, K. Zhang, J. Zhang, B. Yang, and L. Jiang, "The dry-style antifogging properties of mosquito compound eyes and artificial analogues prepared by soft lithography," Adv. Mater. **19**(17), 2213–2217 (2007).
8. K. H. Jeong, J. Kim, and L. P. Lee, "Biologically inspired artificial compound eyes," Science **312**(5773), 557–561 (2006).
9. H. Gao, Z. Liu, J. Zhang, G. Zhang, and G. Xie, "Precise replication of antireflective nanostructures from biotemplates," Appl. Phys. Lett. **90**(12), 123115 (2007).

#139513 - $15.00 USD Received 10 Dec 2010; accepted 1 Feb 2011; published 14 Feb 2011

10. R. J. Martín-Palma, C. G. Pantano, and A. Lakhtakia, "Replication of fly eyes by the conformal-evaporated-film-by-rotation technique," Nanotechnology **19**(35), 355704 (2008).
11. Y.-F. Huang, S. Chattopadhyay, Y.-J. Jen, C.-Y. Peng, T.-A. Liu, Y.-K. Hsu, C.-L. Pan, H.-C. Lo, C.-H. Hsu, Y.-H. Chang, C.-S. Lee, K.-H. Chen, and L.-C. Chen, "Improved broadband and quasi-omnidirectional anti-reflection properties with biomimetic silicon nanostructures," Nat. Nanotechnol. **2**(12), 770–774 (2007).
12. Y. M. Song, S. J. Jang, J. S. Yu, and Y. T. Lee, "Bioinspired parabola subwavelength structures for improved broadband antireflection," Small **6**(9), 984–987 (2010).
13. E. Garnett, and P. Yang, "Light trapping in silicon nanowire solar cells," Nano Lett. **10**(3), 1082–1087 (2010).
14. P. C. Yu, C. H. Chang, C. H. Chiu, C. S. Yang, J. C. Yu, H. C. Kuo, S. H. Hsu, and Y. C. Chang, "Efficiency enhancement of GaAs photovoltaics employing antireflective indium tin oxide nanocolumns," Adv. Mater. **21**(16), 1618–1621 (2009).
15. J. Zhu, C. M. Hsu, Z. Yu, S. Fan, and Y. Cui, "Nanodome solar cells with efficient light management and self-cleaning," Nano Lett. **10**(6), 1979–1984 (2010).
16. M. Ishimori, Y. Kanamori, M. Sasaki, and K. Hane, "Subwavelength antireflection gratings for light emitting diodes and photodiodes fabricated by fast atom beam etching," Jpn. J. Appl. Phys. **41**(Part 1, No. 6B), 4346–4349 (2002).
17. Y. M. Song, E. S. Choi, J. S. Yu, and Y. T. Lee, "Light-extraction enhancement of red AlGaInP light-emitting diodes with antireflective subwavelength structures," Opt. Express **17**(23), 20991–20997 (2009).
18. Y. Li, F. Li, J. Zhang, C. Wang, S. Zhu, H. Yu, Z. Wang, and B. Yang, "Improved light extraction efficiency of white organic light-emitting devices by biomimetic antireflective surfaces," Appl. Phys. Lett. **96**(15), 153305 (2010).
19. J. K. Kim, S. Chhajed, M. F. Schubert, E. F. Schubert, A. J. Fischer, M. Crawford, J. Cho, H. Kim, and C. Sone, "Light-extraction enhancement of GaInN light-emitting diodes by graded-refractive-index indium tin oxide anti-reflection contact," Adv. Mater. **20**(4), 801–804 (2008).
20. D.-S. Liu, T.-W. Lin, B.-W. Huang, F.-S. Juang, P.-H. Lei, and C.-Z. Hu, "Light-extraction enhancement in GaN-based light-emitting diodes using grade-refractive-index amorphous titanium oxide films with porous structures," Appl. Phys. Lett. **94**(14), 143502 (2009).
21. C.-E. Lee, Y.-C. Lee, H.-C. Kuo, T.-C. Lu, and S.-C. Wang, "High-brightness InGaN-GaN flip-chip light-emitting diodes with triple-light scattering layers," IEEE Photon. Technol. Lett. **20**(8), 659–661 (2008).
22. P.-W. Huang, and Y. S. Wu, "Output power of AlGaInP light emitting diode improved by double roughening AlGaInP surfaces," Electrochem. Solid-State Lett. **13**(5), H163–H165 (2010).
23. Y. Kojima, and T. Kato, "Nanoparticle formation in Au thin films by electron-beam-induced dewetting," Nanotechnology **19**(25), 255605 (2008).
24. S. Wang, X. Z. Yu, and H. T. Fan, "Simple lithographic approach for subwavelength structure antireflection," Appl. Phys. Lett. **91**(6), 061105 (2007).
25. M. G. Moharam, and T. K. Gaylord, "Rigorous coupled-wave analysis of planar-grating diffraction," J. Opt. Soc. Am. **71**(7), 811–818 (1981).
26. M. G. Moharam, and T. K. Gaylord, "Three-dimensional vector coupled-wave analysis of planar-grating diffraction," J. Opt. Soc. Am. **73**(9), 1105–1112 (1983).
27. A. B. Shvartsburg, V. Kuzmiak, and G. Petite, "Optics of subwavelength gradient nanofilms," Phys. Rep. **452**(2-3), 33–88 (2007).
28. A. B. Shvartsburg, V. Kuzmiak, and G. Petite, "Polarization-dependent tunneling of light in gradient optics," Phys. Rev. E Stat. Nonlin. Soft Matter Phys. **76**(1), 016603 (2007).
29. W. K. Wang, S. Y. Huang, S. H. Huang, K. S. Wen, D. S. Wuu, and R. H. Horng, "Fabrication and efficiency improvement of micropillar InGaN/Cu light-emitting diodes with vertical electrodes," Appl. Phys. Lett. **88**(18), 181113 (2006).
30. Y.-K. Ee, P. Kumnorkaew, R. A. Arif, H. Tong, H. Zhao, J. F. Gilchrist, and N. Tansu, "Optimization of light extraction efficiency of III-Nitride LEDs with self-assembled colloidal-based microlenses," IEEE J. Sel. Top. Quantum Electron. **15**(4), 1218–1225 (2009).
31. D. E. Aspnes, and A. A. Studna, "Dielectric functions and optical parameters of Si, Ge, GaP, GaAs, GaSb, InP, InAs, and InSb from 1.5 to 6.0 eV," Phys. Rev. B **27**(2), 985–1009 (1983).

1. Introduction

In recent decades, extensive research efforts have been made by scientists and engineers to mimic micro- or nanostructures in nature because of their useful properties, such as the vivid colors of butterfly wings and diatoms [1,2], the self-cleaning ability of lotus leaves [3], and the broadband antireflection of nipple arrays in compound eyes [4,5]. Indeed, the compound eyes of nocturnal insects present a fascinating object for biomimetic studies due to their well-organized structures for light detection with a wide field of view [6]. These surfaces consist of subwavelength structures (SWSs) with a tapered profile on thousands of hexagonal microlens arrays. The former acts as a homogeneous medium with a graded refractive index profile to reduce Fresnel reflection at the surface, and the latter focuses the incident light towards the photoreceptor cells. These hierarchical micro- and nanostructures also show antifogging effects as well as efficient light collection properties [7].

#139513 - $15.00 USD Received 10 Dec 2010; accepted 1 Feb 2011; published 14 Feb 2011

Bioinspired artificial compound eyes, which were successfully demonstrated by Lee et al. [8], have shown optical characteristics that are very similar to those of natural compound eyes; hence, they are regarded as promising candidates for various optical sensors or imaging systems. However, only a few studies have reported on the integration of SWSs across the entire surface of microstructures (MSs) [9,10], and this continues to be a technical challenge. In practical optoelectronic device applications including solar cells, photodetectors, and light-emitting diodes (LEDs), the use of SWSs could play an important role in enhancing the optical efficiency due to their broadband and omnidirectional antireflection properties [11–18]. Unlike solar cells and other photosensitive devices, the light extraction enhancement of LED with SWSs is hindered mainly by the occurrence of total internal reflection (TIR) above the critical angle. This effect accounts for why most LEDs with SWSs or graded index materials show only a ~30% improvement in light output power [16–20].

Herein, we demonstrate bioinspired compound eye surface structures consisting of SWSs on MSs for the purpose of eliminating both Fresnel reflection and total internal reflection in LEDs. The main mechanism for light escaping is quite different with previously reported multi-roughened surface structures [21,22]. The SWSs with desired feature are formed across the entire surface of hexagonally patterned MSs on GaP substrates by an overall dry etch process using thermally dewetted silver (Ag) nanoparticle masks [23,24]. In this approach, the SWSs on MSs provide efficient light extraction and thus improve the light output power by up to 70% in AlGaInP red LEDs as compared to that of conventional LEDs.

2. Compound eye surface structures: Hierarchical micro- and nanostructures

In general, the external quantum efficiencies of AlGaInP-based LEDs are low because the refractive index of the GaP window layer differs greatly from that of air. For conventional LEDs with a flat surface (Fig. 1(a)-i), any light generated from the active layer that propagates in the direction normal to the LED surface experiences an internal Fresnel reflection of ~29% at the interface between the GaP and air. As the incident angle increases from the normal to the critical angle (~17.6°), the Fresnel reflection reaches 100%, which significantly degrades the device performance. Even though the probability of TIR occurrence can be reduced by introducing MSs (Fig. 1(a)-ii) such as microlens arrays, micropillars, and textured surfaces, at least 29% reflection exists at any incident angle. This means that Fresnel reflection at the device surface cannot be removed by the MS. Alternatively, the Fresnel reflection below the critical angle can be effectively reduced by implementing SWSs on the surface (Fig. 1(a)-iii). Figure 1(b) shows the internal reflectance of GaP substrates with and without SWSs as a function of the incident angle at a wavelength of 635 nm, as calculated by a rigorous coupled-wave analysis (RCWA) method [25,26]. In RCWA calculation, the incident light was assumed as plane waves with a fixed polarization angle of 45° instead of randomly polarized light. As shown in Fig. 1(b), a very low reflectance (<5%) is sustained at incident angles of less than 15° for SWS-integrated GaP substrates, but the reflectance still reaches 100% at the critical angle. Because the light propagation in SWSs is quite similar to that in a graded-index medium, the optical path is bent in the SWS region and the light is totally reflected with a certain tunneling depth into the graded-index layer above the critical angle [27,28]. As depicted in Fig. 1(c), the electric field cannot penetrate the SWS region at an incident angle of 20°, while it easily passes through the SWS region without reflection at the normal incident angle. This indicates that SWSs alone cannot handle the TIR. According to these rules, SWSs on a patterned MS (Fig. 1(a)-iv), which are similar to structures on the surfaces of compound eyes, can effectively reduce the Fresnel reflection as well as the TIR.

#139513 - $15.00 USD Received 10 Dec 2010; accepted 1 Feb 2011; published 14 Feb 2011

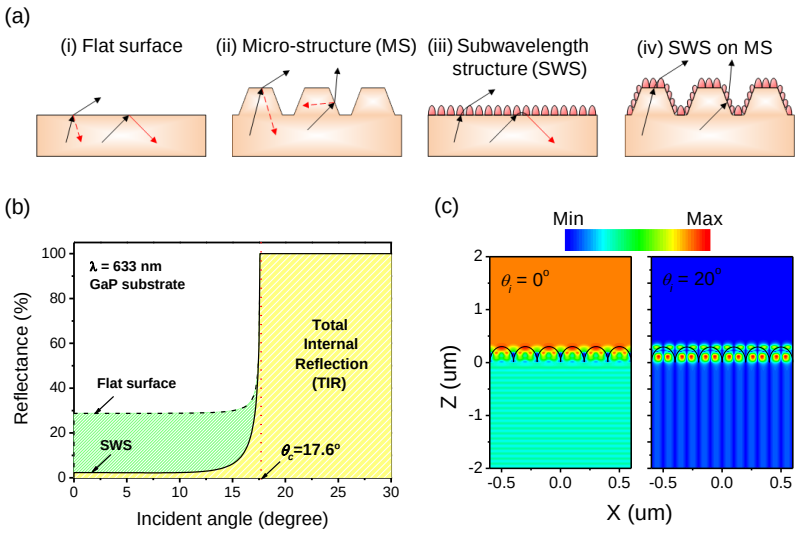

Fig. 1. (a) Schematic diagram of four surface structures: (i) a flat surface, (ii) an MS, (iii) an SWS, and (iv) an SWS on an MS. The dashed and solid red arrows indicate the Fresnel internal reflection and total internal reflection, respectively. (b) Calculated internal reflectance of the GaP substrate with and without an SWS as a function of incident angle at a wavelength of 635 nm. (c) Electric field intensity distribution of the SWS on a GaP substrate at 635 nm for incident angles of 0° and 20°.

3. Fabrication and characterization of artificial compound eye surface structures

In order to demonstrate the proposed structure, we fabricated SWSs integrated onto patterned MSs on a GaP substrate as illustrated in Fig. 2(a). First, hexagonally patterned MSs were fabricated on a single-side-polished GaP wafer by a dry etch process using thermally reflowed photoresist (PR) masks. To create tapered sidewalls, lens-like PR patterns that had been formed by a thermal reflow process on a hot plate were used as an etch mask. For SWS fabrication, Ag thin films with a thickness of 15 nm were deposited across the whole surface by using an e-beam evaporator. Then, a thermal dewetting process was conducted at 500 °C for 1 min via rapid thermal annealing. The Ag film thickness and the dewetting temperature were carefully chosen to form separated Ag nanoparticles (NPs) with an average distance of less than 200 nm [17]. In order to fabricate SWSs with a tapered profile, the underlying GaP layer was etched by using an ICP etcher under optimized conditions. The residual Ag masks were removed by reactive ion etching in a CF_4/O_2 gas mixture. The samples were characterized by using a field-emission scanning electron microscopy (FE-SEM) (S-4700, Hitachi, Japan) with an operating voltage of 10-15 kV. Transmittance and reflectance spectra of the samples were measured by UV/VIS/NIR spectrophotometry (Cary 5000, Varian, USA) in diffuse mode with an integrating sphere.

Figure 2(b) shows SEM images of the fabricated samples with (i) an MS, (ii) an SWS, and (iii) an SWS/MS on a GaP substrate. As can be seen in Fig. 2(b)-iii, there are two geometrical differences between artificial and natural compound eye surface structures. First, the fabricated MS has a diameter of ~2 μm with a 1-μm spacing to increase the outcoupling [29,30], whereas the microlenses of compound eyes in nature have a diameter of ~20 μm. This difference arises from the different intended uses of the structures. Second, the fabricated SWSs are randomly distributed while nipple arrays in nature are organized in hexagonal arrays. However, these structures are sufficient to reduce the surface reflection. A major advantage of thermally dewetted Ag NP masks is that they can form the SWS on a patterned or roughened surface. For most nano-fabrication methods such as e-beam/interference lithography and nanosphere/colloid formation, it is difficult to form nanopatterns on a patterned surface because these methods require a spin-coating process. As shown in Fig.

#139513 - $15.00 USD Received 10 Dec 2010; accepted 1 Feb 2011; published 14 Feb 2011

2(b)-iii, the entire MS-patterned substrate was covered with the SWS. The height and average distance between adjacent cones of the fabricated SWS were approximately 120 nm and 150 nm, respectively, which were chosen by design rules based on the RCWA calculation.

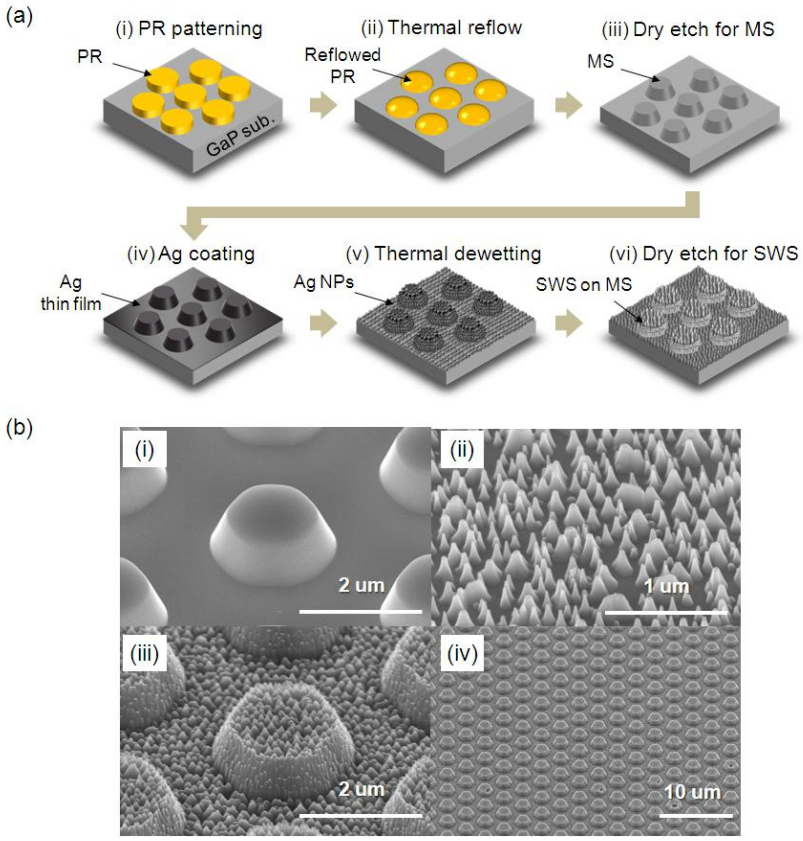

Fig. 2. (a) Schematic illustration of the fabrication procedure for the SWS/MS architecture. (b) Tilted-angle view of SEM images for the fabricated samples with (i) an MS, (ii) an SWS, and (iii) an SWS/MS on a GaP substrate. (iv) A lower magnification image of (iii).

Figure 3(a) shows a contour plot of the variation in reflectance from the SWS on a GaP substrate as a function of the SWS wavelength and period. The height of the SWS was set to 300 nm. At a wavelength of 635 nm, the SWSs with a period of > 250 nm exhibit very high reflectance (>30%) due to higher order diffraction. Figure 3(b) illustrates the electric field intensity distribution of SWSs on a GaP substrate with a period of 200 nm (top) and 300 nm (bottom) at 635 nm for normal incidence. As shown in Fig. 3(b), the SWSs with a 300-nm period block the electric field and reflect it backwards whereas the SWSs with a period of 200 nm enhance the light transmission. The height of the SWS also affects the reflection characteristics. Figure 3(c) shows the reflectance variation of a GaP SWS with a period of 200 nm as a function of the SWS wavelength and height. The period of the SWS was set to 200 nm. As the height is increased, the reflectance tends to decrease. This can be explained by the fact that the effective refractive index changes more gradually at greater heights. These tendencies are also affected by the incident wavelength. For example, the first reflectance dip is found at a height of 150 nm for an incident wavelength of 635 nm, but the first dip appears for a height of 260 nm for the case of a 1000-nm wavelength. Following these rules, we chose to use SWSs with a period below 200 nm and a height above 100 nm to obtain less than 5% reflectance at an incident wavelength of 635 nm.

#139513 - $15.00 USD Received 10 Dec 2010; accepted 1 Feb 2011; published 14 Feb 2011

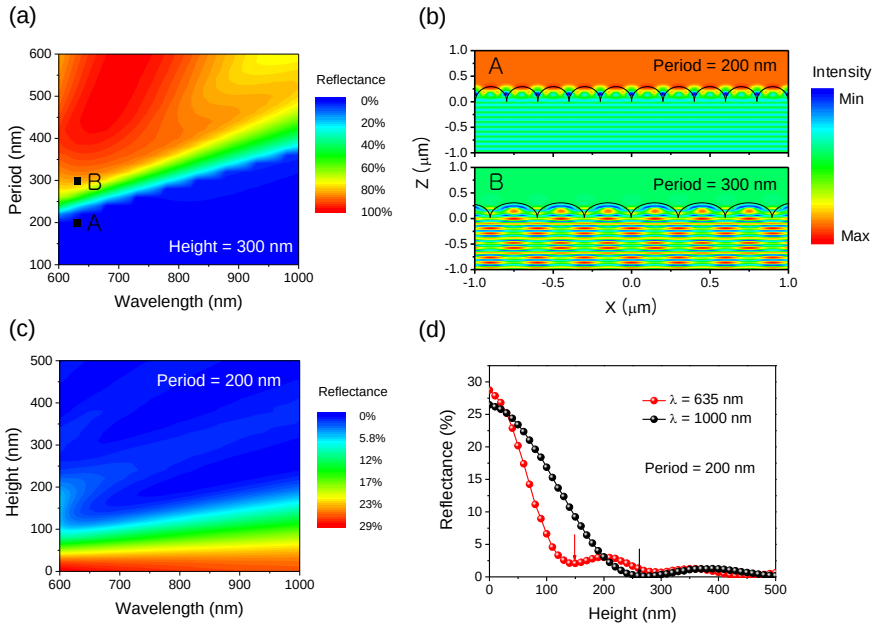

Fig. 3. (a) Contour plot of the reflectance variation of SWSs on a GaP substrate as a function of SWS wavelength and period. The height of the SWS was set to 300 nm. (b) Electric field intensity distribution of SWSs on a GaP substrate with a period of 200 nm (A) and 300 nm (B) at 635 nm for normal incidence. (c) Contour plot of the reflectance variation of a GaP SWS as a function of the SWS wavelength and height. The period of the SWS was set to 200 nm. (d) Reflectance of a GaP SWS with a period of 200 nm as a function of the SWS height at a wavelength of 635 nm (red line) and 1000 nm (black line). Each arrow indicates the first reflectance dip position, i.e., h_{dip} = 150 nm at a wavelength of 635 nm and h_{dip} = 260 nm at a wavelength of 1000 nm.

To investigate the effect of SWS/MSs on light extraction, the transmittance characteristics of GaP substrates with four different surface structures, i.e., a flat surface, an MS, an SWS, and an SWS/MS, were measured at normal incidence, as shown in Fig. 4(a). To induce randomly scattered light, samples with a slightly roughened back-surface were used for the transmittance measurements. For all of the surface structures, there is no transmission at wavelengths below ~540 nm due to strong material absorption [31]. In the range of GaP transparency, the transmittance steadily increases as the wavelength increases because the refractive index of GaP decreases slightly. As depicted in Fig. 4(b), the transmittances of the MS and the SWS are improved by similar ratios as compared to that of the flat surface, and the average enhancement ratios in the range of 600 to 800 nm are 19.35% and 16.23%, respectively. By merging the effects of the MS and the SWS, the transmittance is significantly enhanced with an average enhancement ratio of 30.41%.

Figure 4(c) shows the measured total reflectance of GaP substrates with four different surface structures, i.e., a flat surface, an MS, an SWS, and an SWS on an MS, at the normal incidence angle in diffuse mode with an integrating sphere. For all of the samples, a rapid increase in reflectance exists above λ~550 nm. This is caused by the backscattering of light due to reflection from the back-surface of the GaP substrate. For a bulk GaP substrate, the reflectance is very high (>~30%) at wavelengths of 300-800 nm. The reflectance is slightly reduced for MS-patterned GaP as compared to the bulk GaP substrate due to the increased surface area. Alternatively, the reflectance from the SWS integrated onto a GaP substrate is significantly reduced because of the strong reduction of Fresnel reflection. By combining a SWS and an MS, the reflectance is even further reduced, as expected. This improved antireflection property could be applied to photovoltaic devices to improve the light absorption efficiency.

#139513 - $15.00 USD
Received 10 Dec 2010; accepted 1 Feb 2011; published 14 Feb 2011

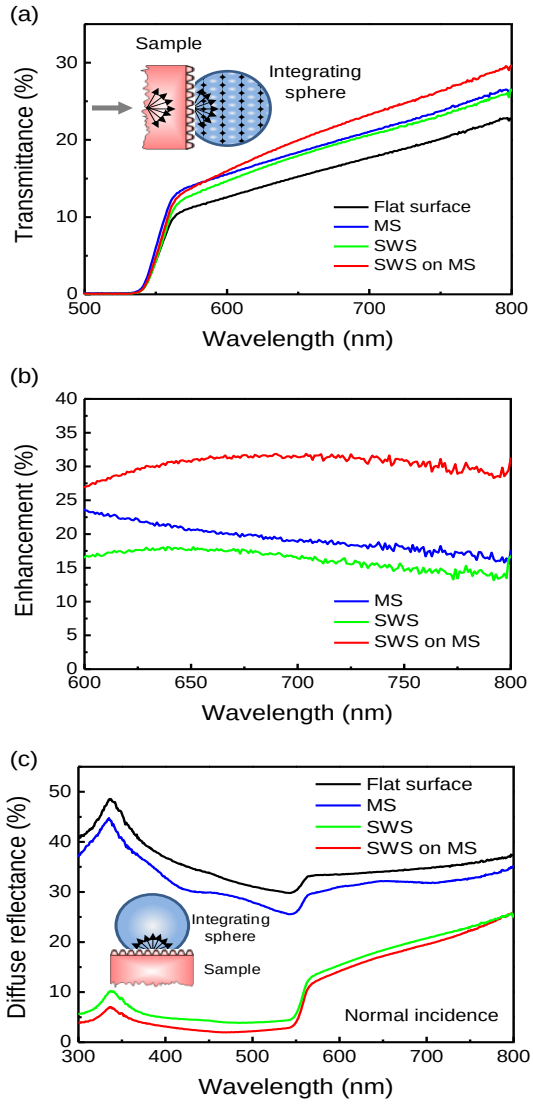

Fig. 4. (a) Measured total transmittance of backside illuminated light as a function of wavelength for a GaP substrate with four different surface structures (a flat surface, a MS, a SWS, and an SWS on an MS). To induce randomly diffused light, samples with a slightly roughened back-surface were used. (b) Transmittance enhancement ratio of each sample as measured against a reference sample with a flat surface. (c) Measured total reflectance of GaP substrates with four different surface structures at normal incidence in diffuse mode with an integrating sphere.

4. Artificial compound eye surface structures on AlGaInP LEDs

To confirm the viability of this proposed structure, red AlGaInP LEDs (λ = 635 nm) with SWS/MSs were fabricated by combining the conventional fabrication method for AlGaInP LEDs and the SWS/MS process, as illustrated in Fig. 5. To define a hexagonally patterned MS on the LED surface, PR patterns with a diameter of 2 μm and a thickness of ~600 nm were formed on the LED surface without a metal pad region (Fig. 5-i) by using a conventional lithography process. After developing, the thermal reflow process was carried out on a hotplate at 200 °C for 1 min to make a lens-like PR shape, which enables a tapered etch

#139513 - $15.00 USD Received 10 Dec 2010; accepted 1 Feb 2011; published 14 Feb 2011

profile. Subsequently, a dry etch process was conducted using an ICP etcher to form the MS (Fig. 5-ii). A $SiCl_4$/Ar (7.5/2.5 sccm) gas mixture at a process pressure of 2 mTorr was used, and the RF and ICP powers were 100 W and 50 W, respectively. For p- and n-ohmic contacts, AuBe/Au (80 nm/500 nm) and Ni/Au/Ge/Ni/Au (20 nm/100 nm/50 nm/30 nm/500 nm) metal layers were deposited on the p-GaP layer and the backside of the wafer, respectively, by using an e-beam evaporator (Fig. 5-iii). Each device had dimensions of 400 μm x 400 μm and was etched down to the n-GaAs substrate to isolate the devices by using an ICP etcher.

To fabricate the SWS on the MS-patterned LED surface, an Ag thin film was deposited on the LEDs by an e-beam evaporator at a deposition rate of 1 Å/s (Fig. 5-iv). A thermal dewetting process was carried out at 500 °C for 1 min under a nitrogen atmosphere by using a rapid thermal process system (Fig. 5-v). The annealing temperature was chosen to reduce the ohmic resistance and to form separated Ag NPs with an adequate average distance. To form the SWS with a tapered profile, the underlying MS-patterned LED surface was etched by using an ICP etcher under optimum conditions, i.e., $SiCl_4$/Ar (7.5/30 sccm) with an RF power of 150 W for 4 min. The residual Ag masks were removed by CF_4/O_2 reactive ion etching.

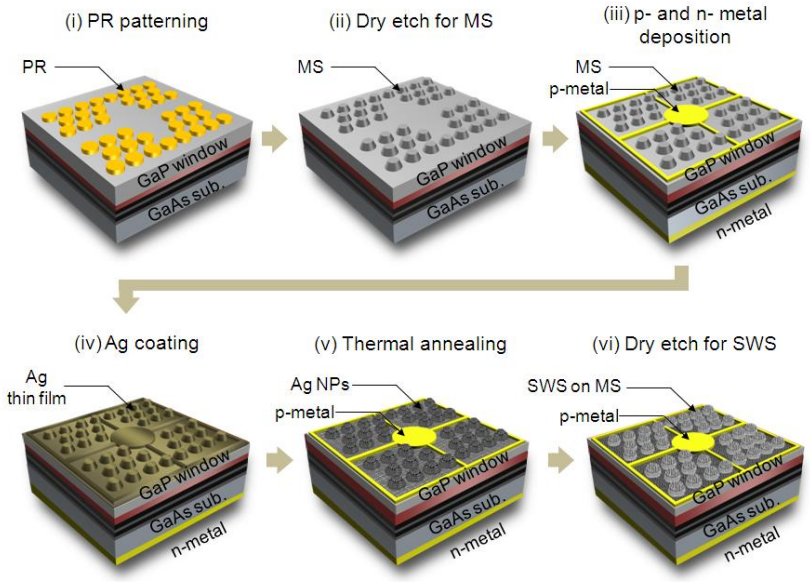

Fig. 5. Schematic illustration of the fabrication procedure for SWS/MS-integrated AlGaInP LEDs.

For comparison, AlGaInP LEDs with a flat surface (conventional device), a MS alone, and an SWS alone were also fabricated. Figure 6(a) shows SEM images of the fabricated SWS/MS-integrated LEDs. All characterizations were carried out at the wafer level at room temperature. The light output power from the top of the LEDs was measured by a large-size silicon photodetector (10 mm × 10 mm) in close proximity to the device. Figure 6(b) shows the light-current-voltage (L-I-V) curves of the fabricated LEDs with four different surface structures. In the four different devices, the forward voltage ranged from 2.24 V to 2.45 V at a bias current of 100 mA. For the LED with the SWS/MS, there is a slight increase in the forward voltage caused by the roughened surface; this does not, however, result in a serious degradation of the electrical properties of the LED. The light output power was improved over that of conventional LEDs by 35.91%, 32.82%, and 72.47% at a bias current of 100 mA for the LEDs with an MS, an SWS, and an SWS/MS, respectively. The improvement of the light extraction is attributed to the elimination of Fresnel reflection by the SWS and the reduction of TIR by the MS. Further improvements in light output power can be achieved by the geometrical optimization of the MS together with the SWS.

#139513 - $15.00 USD Received 10 Dec 2010; accepted 1 Feb 2011; published 14 Feb 2011

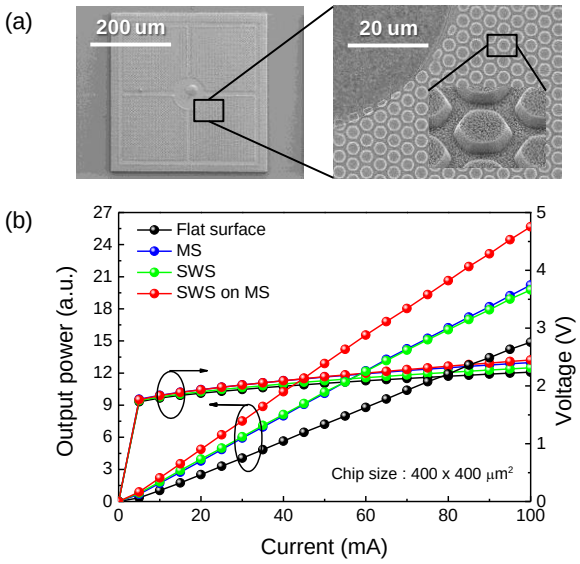

Fig. 6. (a) SEM images of the fabricated LEDs with SWS/MSs. (b) L-I-V curves of the fabricated LEDs with four different surface structures: flat surface, MS, SWS, and SWS/MS.

5. Conclusion

In summary, we have proposed bioinspired artificial compound eye surface structures by integrating SWSs and MSs; these structures eliminate Fresnel reflection and total internal reflection as predicted by theoretical calculations. As a proof of this concept, SWS/MSs on a GaP substrate were fabricated by simple process steps, and a transmittance enhancement of 30.41%, as compared to that of a flat surface, was demonstrated. To demonstrate an optoelectronic device application, it was also shown experimentally that AlGaInP LEDs with a SWS/MS achieved a 72.47% enhancement in light output power over conventional LEDs without any degradation of the electrical characteristics. This striking effect could be highlighted even further in white light-emitting devices and materials with broad wavelength spectra and photovoltaic devices because of their broadband antireflection properties. Hence, we believe that artificial compound eye structures have considerable potential for future low-cost and high-efficiency optical device applications.

Acknowledgements

This work was partially supported by the GIST Systems Biology Infrastructure Establishment Grant, by the World Class University (WCU) program at GIST through a grant provided by MEST of Korea (R31-20008-000-10026-0) and by the Core Technology Development Program for Next-Generation Solar Cells of Research Institute for Solar and Sustainable Energies (RISE), GIST.